

Accepted version on Author's Personal Website: C. R. Koch

Article Name with DOI link to Final Published Version complete citation:

David Gordon, Christian Wouters, Maximilian Wick, Bastian Lehrheuer, Jakob Andert, Charles R Koch, and Stefan Pischinger. Development and experimental validation of a field programmable gate array-based in-cycle direct water injection control strategy for homogeneous charge compression ignition combustion stability. *International Journal of Engine Research*, 0(0):1–12, 2019. doi: <https://doi.org/10.1177/1468087419841744>

See also:

https://sites.ualberta.ca/~ckoch/open_access/Gorden2019.pdf

Post-print

As per publisher copyright is ©2019



This work is licensed under a
[Creative Commons Attribution-NonCommercial-NoDerivatives 4.0 International License](https://creativecommons.org/licenses/by-nc-nd/4.0/).



Article accepted version starts on the next page →

[Or link: to Author's Website](#)

Development and experimental validation of a field programmable gate array-based in-cycle direct water injection control strategy for homogeneous charge compression ignition combustion stability

International J of Engine Research

1–13

© IMechE 2019

Article reuse guidelines:

sagepub.com/journals-permissions

DOI: 10.1177/1468087419841744

journals.sagepub.com/home/jer



David Gordon¹ , Christian Wouters² , Maximilian Wick³ , Bastian Lehrheuer², Jakob Andert³ , Charles Koch¹ and Stefan Pischinger²

Abstract

Homogeneous charge compression ignition is a part-load combustion method, which can significantly reduce oxides of nitrogen (NO_x) emissions compared to current lean-burn spark ignition engines. The challenge with homogeneous charge compression ignition combustion is the high cyclic variation due to the lack of direct ignition control. A fully variable electromagnetic valve train provides the internal exhaust gas recirculation through negative valve overlap which is required to obtain the necessary thermal energy to enable homogeneous charge compression ignition. This also increases the cyclic coupling as residual gas and unburnt fuel is transferred between cycles through exhaust gas recirculation. To improve combustion stability, an experimentally validated feed-forward water injection controller is presented. Utilizing the low latency and rapid calculation rate of a field programmable gate array, a real-time calculation of residual fuel mass is implemented on a prototyping engine controller. Using this field programmable gate array-based calculation, it is possible to calculate the amount of fuel and the required control interaction during an engine cycle. This controller prevents early rapid combustion following a late combustion cycle using direct water injection to cool the cylinder charge and counter the additional thermal energy from any residual fuel that is transferred between cycles. By cooling the trapped cylinder mass, the upcoming combustion phasing can be delayed to the desired setpoint. The controller was tested at several operating points and showed an improvement in the combustion stability as shown by a reduction in the standard deviation of combustion phasing and indicated mean effective pressure.

Keywords

Homogeneous charge compression ignition, gasoline-controlled autoignition, in-cycle control, direct water injection, field programmable gate array, real-time modeling

Date received: 31 October 2018; accepted: 5 March 2019

Introduction

Homogeneous charge compression ignition (HCCI) is a part-load combustion method, which is characterized by lean low-temperature combustion (LTC). HCCI has the potential to significantly reduce NO_x emissions by as much as 99% when compared with current stratified lean-burn gasoline combustion.^{1–3} Therefore, expensive exhaust after-treatment systems can be reduced or simplified.^{4–6} HCCI utilizes rapid multi-site combustion, and this in combination with reduced wall heat losses from LTC leads to thermodynamic and fuel efficiency benefits of up to 30% over current gasoline engines.⁷ HCCI combustion is defined by compression-induced

autoignition and is therefore highly dependent on the in-cylinder temperature, pressure and fuel mixture after compression. The lack of a direct combustion timing

¹Department of Mechanical Engineering, University of Alberta, Edmonton, AB, Canada

²Institute for Combustion Engines, RWTH Aachen University, Aachen, Germany

³Mechatronic Systems for Combustion Engines, RWTH Aachen University, Aachen, Germany

Corresponding author:

David Gordon, Department of Mechanical Engineering, University of Alberta, Edmonton, AB T6G 2R3, Canada.

Email: dgordon@ualberta.ca

control method like spark timing in spark ignition (SI) engines or injection timing in traditional compression ignition (CI) engines is a major challenge of this combustion method.

Ignition timing is strongly dependent on temperature and can be altered through intake air heating, increased compression ratio or exhaust gas recirculation (EGR).^{8–11} When using internal EGR as a means to provide the thermal energy required to achieve auto-ignition, a strong coupling between cycles can exist when the engine is operated near the misfire limit.^{12,13} Current cycle-based control strategies only stabilize a small section of the operation range, which is insufficient for practical engine deployment.¹⁴ Therefore, a stabilizing controller which works over a wide range of operating conditions is needed to reduce the cyclic variations in combustion phasing and load, and prevent a spontaneous shift from stable to unstable operation. Previous work in this area has been investigated in the literature.^{4,15–19}

To capture the behavior of HCCI combustion, various simulation models including stochastic, multi-zone and physical models have been developed to predict the gas exchange and combustion processes.^{20–23} Detailed physical models are typically too computationally intensive for use in real-time engine applications and are often linearized around a specific operating point for implementation in processor-based engine controllers.^{24,25} However, using the low latency and parallel computing architecture of field programmable gate array (FPGA) hardware, complex cylinder pressure analysis and control algorithms can be implemented in real time.²⁶ FPGA-based controllers have been successfully used to provide closed-loop control for the position of pneumatic valves.²⁷ An online calculation of heat release²⁸ on FPGA hardware has been used for engine control to calculate unburned fuel and prevent an overshoot of indicated mean effective pressure (IMEP).²⁹ FPGA hardware has also been used to implement a physics-based gas exchange model that is used to calculate the cylinder state including in-cylinder pressure, temperature and trapped mass each 0.1 °CA.³⁰ This FPGA model has been expanded in this work and is used for in-cycle water injection control.

This article will present the development and experimental validation of an FPGA-based in-cycle feed-forward water injection controller. To prevent the early rapid combustion following a late ignition or misfire, water injection is used. The residual fuel mass calculation by Wick et al.²⁹ is improved by incorporating a real-time gas exchange model³⁰ to capture the fuel leaving through the exhaust flow. Correlations between in-cylinder residual fuel mass and combustion phasing will be presented and used to determine the quantity of water injection. Two separate injection timings have been identified as having the largest impact for the injected water mass. Using these two water injection

Table 1. Single-cylinder research engine parameters.

Parameter	Value
Displacement volume	0.499 L
Stroke	90 mm
Bore	84 mm
Compression ratio	12:1
No. of valves (In/Ex)	2/2
Valve train	EMVT
Max. valve lift (In/Ex)	8 mm/8 mm
Valve angle (In/Ex)	22.5°/22.5°
Valve diameter (In/Ex)	32 mm/26 mm
Intake air pressure	1013 mbar
Exhaust pressure	1013 mbar
Oil and coolant temperature	90 °C
Engine speed	1500 L/min
Fuel rail pressure	100 bar
Intake temperature	50 °C

EMVT: electromagnetic valve train.

timings, the control method will be experimentally evaluated and an improvement in HCCI combustion stability will be shown.

Experimental setup

A single-cylinder research engine (SCRE) outfitted with a fully variable electromagnetic valve train (EMVT) is used for all reported results. The EMVT system allows for engine operation with a variety of valve strategies to provide combustion chamber EGR; however, in this work, only negative valve overlap (NVO) will be used to provide the required thermal energy for HCCI combustion. The piston used in the engine has enlarged valve pockets to provide free running operation at any valve timing.

Fuel is injected into the SCRE through a piezoelectric outward-opening hollow-cone injector. The fuel pressure can be varied and is set at 100 bar. The fuel used for all tests in this work is conventional European Research Octane Number (RON) 96 gasoline containing 10% ethanol. For the injection of distilled water directly into the combustion chamber, an identical injector is used. An injection pressure of 50 bar is used throughout this work as it ensures evaporation of the water while still allowing small water injection amounts. The engine geometry and testing conditions are listed in Table 1.

In-cylinder pressure is measured using a Kistler A6061B piezoelectric pressure transducer. The intake and exhaust manifold pressures are measured using Kistler 4045-A5 piezoresistive pressure transducers. Kistler charge amplifiers are used to output the measured pressure as a 0–10 V signal. The positions of the valves are measured using FEV Europe GmbH conductive lift measurement sensors. The angular position of the crank is measured using a 0.1 °CA resolution

Table 2. Rapid prototyping ECU specifications.

	Parameter	Specification
Processor	dSPACE® 1401	IBM PPC-750GL
	Speed	900 MHz
	Memory	16 MB main memory
I/O board	dSPACE® 1513	
	Analog input	24 parallel channels
	Resolution	16 bit
	Sampling	1 MHz
	Analog input	32 multiplexed channels
	Resolution	16 bit
	Sampling	200 kHz
	Analog output	12 channels
	Digital input	40 channels
	Digital output	40 channels
FPGA	dSPACE® 1514	Xilinx® Kintex-7
	Flip-flops	407,600
	Lookup table	203,800
	Memory lookup table	64,000
	Block RAM	445
	Digital signal processing	840
	I/O	478

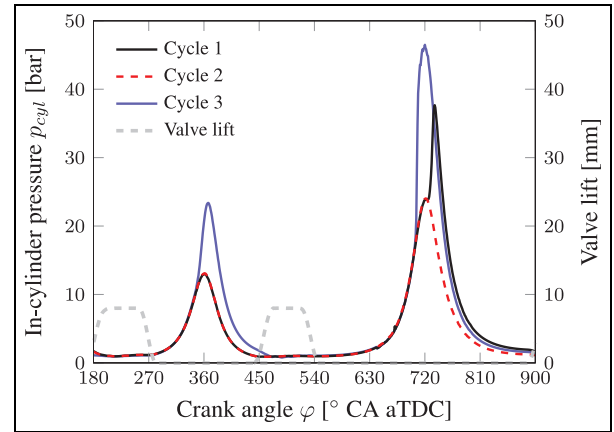
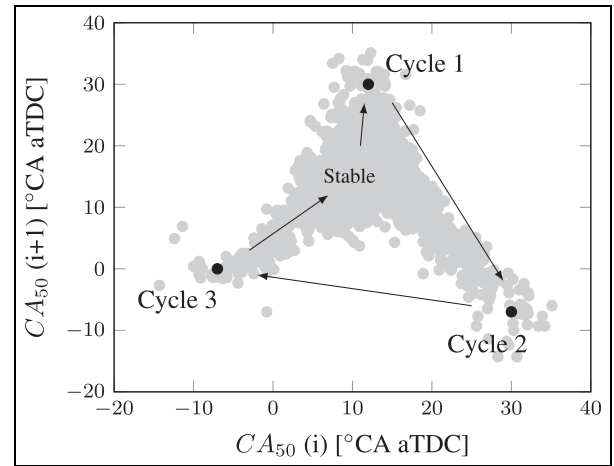
FPGA: field programmable gate array.

optical encoder. All of these signals are simultaneously input into both the combustion analysis system (CAS) and prototyping engine control unit (ECU).

For offline analysis, an FEV CAS is used to record the cylinder and manifold pressures and the valve position at a 0.1°CA resolution. The ECU contains a microprocessor and an FPGA board which are used for real-time gas exchange calculation and engine control. Both injectors and the EMVT system are directly controlled by the FPGA board allowing for rapid control intervention. The control algorithms that are developed are run on the FPGA board along with existing calculations with a sampling time of 12.5 ns on the FPGA used. These additional calculations include a thermodynamic zero-point correction for cylinder pressure referencing. Along with a cylinder pressure indication system and angle calculation module as presented by Pfluger et al.²⁶ For all the tests in this work the processor in the ECU has a sampling time which is set at 0.5 ms. Details of the MicroAutoBox II (MABX) prototyping ECU are provided in Table 2.

Control strategy and combustion phasing correlations

To improve HCCI combustion stability, large cyclic variations need to be reduced. Figure 1 shows the experimentally measured cyclic pressure signals of three consecutive cycles. Cycle 1 is a good representation of a standard cycle with a normal combustion phasing of 12°CA after top dead center of the power stroke (aTDC). It is then followed by cycle 2 which can be considered an incomplete combustion with a very late combustion phasing. Then, due to the incomplete

**Figure 1.** Distinct cyclic variation in the in-cylinder pressure p_{cyl} trace at $n = 1500$ L/min and IMEP = 4.0 bar.**Figure 2.** Distinct cyclic variation in the corresponding combustion phasing CA_{50} return map at $n = 1500$ L/min and IMEP = 4.0 bar.

combustion, residual fuel is transferred to the next cycle through internal EGR. As the combustion phasing is very late, the in-cylinder temperature increases which increases the temperature of the exhaust gas transferred to cycle 3. There is also the possibility that during the NVO recompression a portion of the residual fuel ignites (as seen in cycle 3) and leads to a further temperature increase of the residual exhaust gas. The result is an increase in the temperature of the fresh air charge and the temperature after compression. This leads to an early combustion phasing with a high pressure rise rate. An early combustion phasing is not desired as the high pressure rise rate leads to increased combustion noise and possible engine damage.^{31,32} Overall, high cyclic variation of combustion also tends to reduce thermal efficiency and increase exhaust emissions.³³

Figure 2 shows the return map for the combustion phasing, CA_{50} . A return map is used to show the relationship between the combustion phasing of the current cycle, $CA_{50}(i)$, and of the following one, $CA_{50}(i + 1)$.

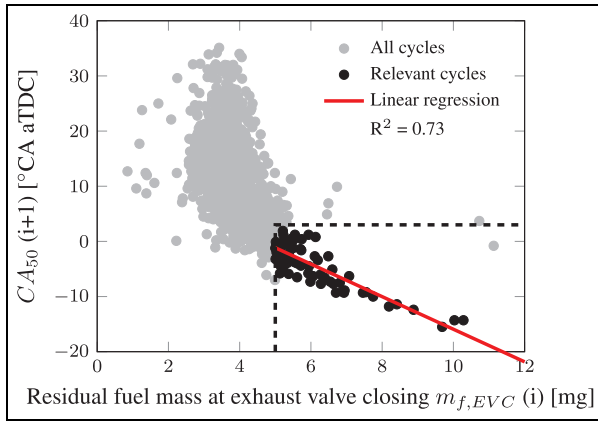


Figure 3. Linear regression of combustion phasing CA_{50} based on residual fuel mass at EVC. Here, $n = 1500$ L/min, IMEP = 4.5 bar, single fuel injection at IVO and $m_{f,injected} = 16.1$ mg.

In the stable operation, two consecutive cycles are not correlated and the return map shows random scatter around the combustion phasing mean. The spread of the data points represents the stochastic variation from cycle to cycle.¹² However, when a distinct pattern or branching can be seen on the return map as is the case in Figure 2, a direct coupling between cycles exists. To effectively stabilize combustion, the spread of the data points and distinct “V” should be reduced.

In this work, cyclic variation will be reduced by preventing the early combustion following a late combustion (cycle 2 in Figure 2) using direct water injection to cool the trapped exhaust gas to retard combustion phasing back to the desired value. The combustion phasing as a function of the residual fuel mass at exhaust valve closing (EVC) is shown in Figure 3 where a strong relationship between a high residual fuel mass and an early combustion phasing is apparent. The cycle with an early phasing can be seen as a leg extending out of the main point cloud. The relevant cycles were chosen by selecting a combustion phasing cutoff of 2 °CA and a residual fuel mass of 5 mg. These limits were manually selected to capture the cycles with a clear trend from the main point cloud. A linear regression is performed to provide a relationship between combustion phasing and residual fuel mass for these cycles. Using the residual fuel mass as the control variable, the model is physically based and is better able to handle changes in valve timing and boost pressure for a wider operating range and better disturbance rejection.

Impact of direct water injection

To evaluate the influence of water injection timing, the start of injection (SOI) was varied between 270 °CA and 720 °CA aTDC. The amount of injected water was kept constant at 2.3 mg, which is the smallest possible

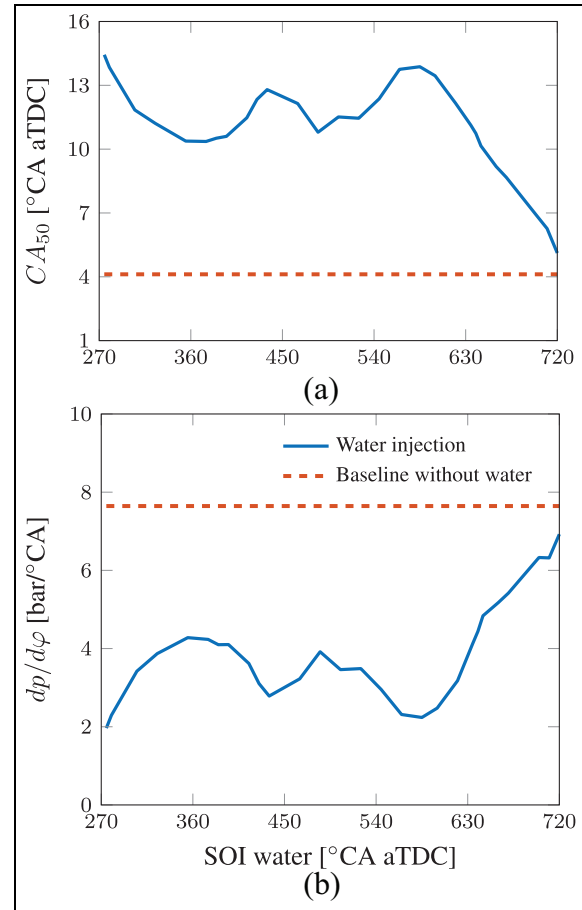


Figure 4. Effect of water injection timing on (a) pressure rise rate and (b) combustion phasing when $n = 1500$ L/min, NVO = 166 °CA, IMEP = 4.5 bar, $(p_{inj} - p_{cyl}) = 50$ bar, $m_{H_2O} = 2.3$ mg and $t_{inj,H_2O} = 0.1$ ms.

injection duration for the injector used. The pressure difference between the water rail and cylinder pressure at the point of injection was maintained at 50 bar to ensure good water evaporation while keeping the pressure low to limit the amount of injected water. The resulting combustion phasing is shown in Figure 4(a) with the corresponding peak pressure rise rate shown in Figure 4(b). As the combustion phasing timing is delayed, the pressure rise gradient also decreased as the piston is already moving downward which is the expected relationship between combustion phasing and pressure gradient.

To increase the effect of water injection and reduce the amount of water needed, there are two points where the largest impact of water can be achieved. These points are early in the compression at 270 °CA and 580 °CA aTDC. The next step is to determine the sensitivity of combustion timing to the injected water mass using these two injection timings that achieve the largest delay in CA_{50} . Variation of injected water mass at constant engine speed is performed and shown in Figure 5. An approximately linear relationship between the

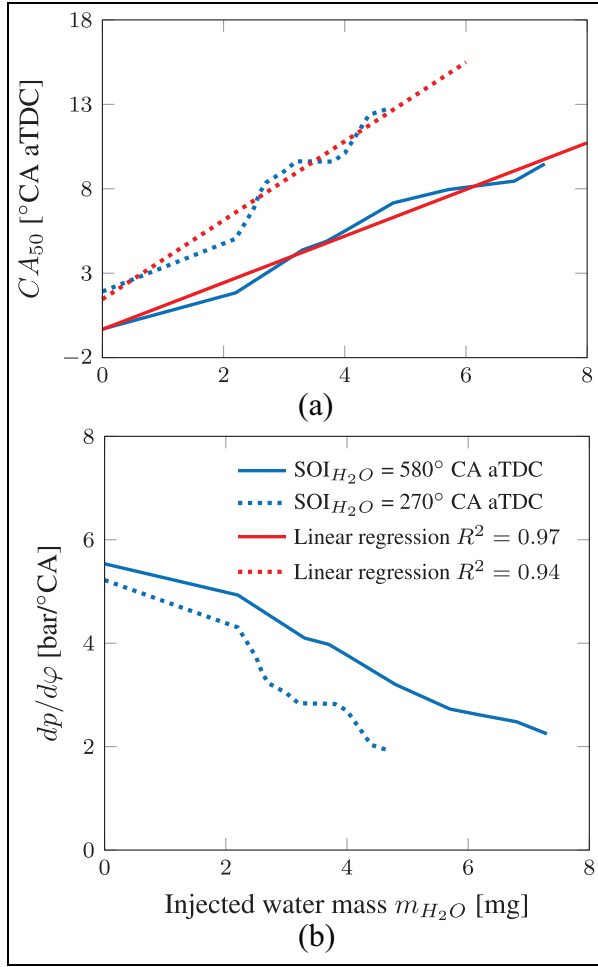


Figure 5. Effect of water injection amount on (a) pressure rise rate and (b) combustion phasing when $n = 1500$ L/min, NVO = 172° CA, IMEP = 4.0 bar and $(p_{inj} - p_{cyl}) = 50$ bar.

injected water mass and the change in combustion phasing and pressure rise gradient is observed. The angle of combustion phasing retards due to injected water mass which is then fit with a linear regression as shown in Figure 5. This linear fit is used to determine the required amount of water to inject based on the prediction combustion phasing of the upcoming cycle.

FPGA timing constraint

The correlations presented relate residual fuel mass at EVC to injected water mass at one of the optimal injection timings. Since one injection timing is at EVC, it is necessary to have a real-time capable calculation of both the residual fuel mass and the injection controller. To do this, an FPGA is used for the implementation of the calculation to ensure that the water injection can begin shortly after EVC. In the tests performed, the desired EVC timing is set at 268° CA aTDC and the water injection is started at 270° CA aTDC, leaving 2° CA between events to ensure that the EMVT is completely closed. This limits the calculation time to 0.22 ms at an engine speed of 1500 L/min. This is too

short for the existing microprocessor in the ECU but is easily handled by the FPGA-based controller which is able to complete the residual fuel mass and injection controller calculations within 0.1° CA. This could allow for the water injection to begin even closer to EVC for an engine with a traditional valve train.

For the water injection starting at 580° CA aTDC, the same FPGA injection controller is used. This is not necessary for the water control as 312° CA is available for the calculation of an injected water mass. However, the real-time calculation of the residual fuel mass still needs to be calculated by the FPGA as a larger time step would introduce resolution errors.³⁰

Real-time residual fuel mass calculation

To achieve the fast calculation times needed for in-cycle control, the calculation of residual fuel mass was ported to the FPGA board in the prototyping ECU. Previous work on a residual fuel mass calculation²⁹ was expanded by removing lookup tables to capture cyclic variations and including a real-time capable zero-dimensional physics-based gas exchange model with a calculation of in-cylinder temperature, mass and gas properties.³⁰

The heat release from combustion is determined from the first law of thermodynamics. The change in crank angle ϕ is related to the time domain via $d\phi = \omega dt$ where ω is the angular engine velocity. Using the energy conservation law for the cylinder, while neglecting kinetic energy and the latent heat of fuel evaporation, yields:

$$\frac{dU}{d\phi} + \frac{dQ_b}{d\phi} = \frac{dQ_w}{d\phi} - p \frac{dV}{d\phi} + \sum_i h_i \frac{dm_i}{d\phi} \quad (1)$$

where $dU/d\phi$ is the internal energy change, $dQ_b/d\phi$ is the fuel energy release, $dQ_w/d\phi$ is the wall heat transfer, $p dV/d\phi$ is the internal work and $h_i dm_i/d\phi$ is the intake and exhaust enthalpy flows.

To calculate the heat release, it is assumed that, for both the high pressure and NVO recompression phase, no mass flows out of the cylinder since the valves are closed. Additional simplifications of equation (1) can be made by neglecting the blow-by mass flow³⁴ and assuming that the mixture preparation takes place before the start of combustion, which yields

$$\frac{dQ_b}{d\phi} = -mc_v(T) \frac{dT}{d\phi} + \frac{dQ_w}{d\phi} - p \frac{dV}{d\phi} \quad (2)$$

Then, by considering the differential form of the thermodynamic equation of state for ideal gases, $pV = mRT$, and substituting into equation (2) yields

$$\begin{aligned} \frac{dQ_b}{d\phi} = & -\frac{c_v(T)}{R} \left(V \frac{dp}{d\phi} - mT \frac{dR}{d\phi} \right) \\ & - \left(1 + \frac{c_v(T)}{R} \right) p \frac{dV}{d\phi} + \frac{dQ_w}{d\phi} \end{aligned} \quad (3)$$

Assuming a constant gas composition $dR/d\varphi = 0$ and using the relations $R = c_p - c_v$ and $\gamma = c_p/c_v$, the rate of heat release can be further simplified to

$$\frac{dQ_b}{d\varphi} = -\frac{1}{\gamma-1}V\frac{dp}{d\varphi} - \frac{\gamma}{\gamma-1}p\frac{dV}{d\varphi} + \frac{dQ_w}{d\varphi} \quad (4)$$

To calculate the wall heat transfer, both the spatially averaged gas temperature in the cylinder $T(\varphi)$ and wall temperature T_w are required. For this work, the wall temperature is assumed constant ($T_w = 465$ K) over an entire cycle and the charge temperature can be obtained from the equation of state (equation (1)). The wall heat transfer can then be expressed as

$$\frac{dQ_w}{d\varphi} = \alpha(\varphi)A(\varphi)(T_w - T(\varphi)) \quad (5)$$

Various methods to calculate wall heat transfer coefficient $\alpha(\varphi)$ are given in the literature.^{35–37} For HCCI combustion, the Hohenberg correlation is often used³⁸ and is

$$\alpha(\varphi) = 130V^{-0.06}p^{0.8}T^{-0.4}(\nu_{pis} + 1.4)^{0.8} \quad (6)$$

The piston speed ν_{pis} in equation (6) is calculated as a function of crank angle $\nu_{pis}(\varphi)$.

Then, using the measured pressure and the calculated cylinder volume and temperature from the existing gas exchange model,³⁰ the integration of the rate of heat release for the duration of combustion yields the heat release as a function of crank angle

$$Q_b(\varphi) = \int_{\varphi_{SOC}}^{\varphi_{EOC}} dQ_b(\varphi) \quad (7)$$

The calculated heat release during the main and NVO compression is used to calculate the amount of fuel mass m_f reacting in the combustion chamber at any point throughout the cycle. The combustion of fuel during the main combustion and NVO recompression can be obtained from the respective heat release Q_b and the lower heating value (LHV) of the fuel

$$m_{f,b} = \frac{Q_b}{LHV} \quad (8)$$

The conversion of fuel during combustion and portion of unburned fuel leaving through the exhaust should be subtracted from the injected fuel mass $m_{f,inj}$

$$m_f = m_{f,inj} - m_{f,b,main} - m_{f,ex} - m_{f,b,NVO} \quad (9)$$

The unburned fuel mass leaving via the exhaust $m_{f,ex}$ is determined by assuming that the residual fuel is homogeneously distributed in the exhaust gas and can be determined by the mass fraction of exhaust gas x_{ex} multiplied by the residual fuel mass at exhaust valve opening (EVO) $m_{f,EVO}$

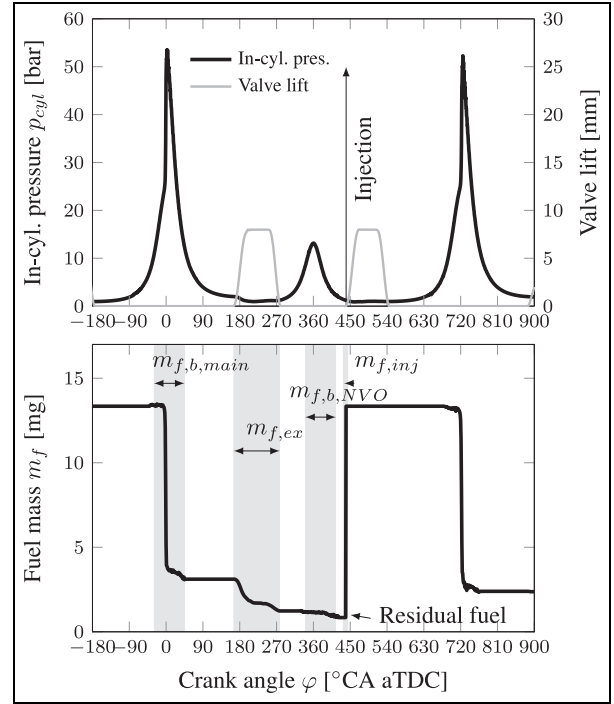


Figure 6. Real-time residual fuel mass calculation.

$$m_{f,ex} = \frac{m_{cyl,EVO} - m_{cyl,EVC}}{m_{cyl,EVO}} m_{f,EVO} \quad (10)$$

$$= x_{ex} m_{f,EVO}$$

in which the exhaust gas fraction x_{ex} is defined as the fraction of the total in-cylinder mass leaving the combustion chamber. The implementation of fuel mass calculation yields continuous crank angle-resolved information about the current fuel mass present in the combustion chamber as shown in Figure 6. Residual fuel transferred from previous cycles can now be calculated.

Controller implementation

By combining the real-time residual fuel mass calculation with the correlation between residual fuel mass and combustion phasing (shown in Figure 3), a feed-forward controller can be implemented to control combustion phasing of the cycle following a late combustion by injecting water. The linear regressions for both the combustion phasing correlation and the water injection mass correlation allow for extrapolation outside of the data range presented in Figures 3 and 5, respectively. The final controller output is then restricted for small water injection amounts to the minimum water injection of 2.2 mg H₂O. The control output is also limited to 15 mg H₂O to provide a reasonable upper limit on the injection duration; however, this limit was never hit during testing but provided a restriction to prevent excessive water injection amounts. As described earlier, the most efficient water injection (for CA₅₀ delay) is

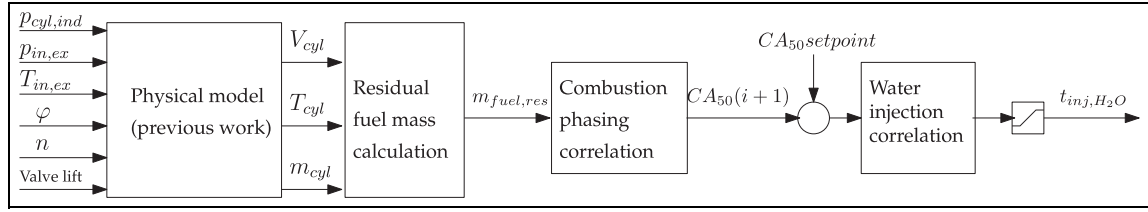


Figure 7. Schematic overview of water injection control strategy.

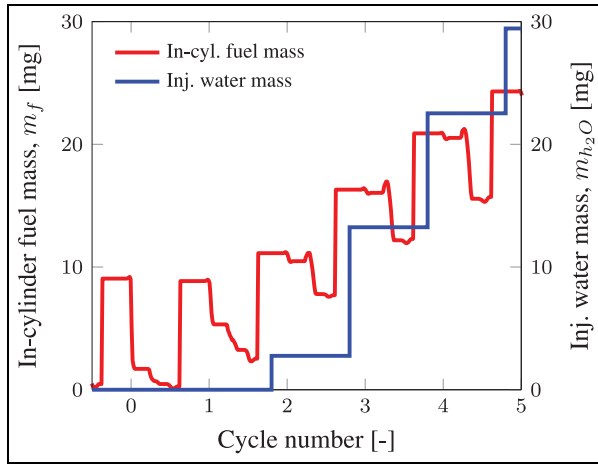


Figure 8. Growth of water injection amount resulting in complete HCCI extinction.

270 °CA or 580 °CA aTDC. Both timings will be tested in this work. The overall control strategy is shown schematically in Figure 7.

The implementation of the proposed controller takes place on the FPGA side of the ECU along with the existing gas exchange model.³⁰ Therefore, the complete calculation takes place within 0.1 °CA. The relative simplicity of the controller presented allows for the combustion phasing and water mass correlations along with the calculation of the start and end angles of water injection to be calculated in 28 FPGA samples (or 350 ns for the FPGA used in this study). This controller utilizes very little additional FPGA resources when compared to the existing gas exchange model³⁰ with the proposed controller consuming below 1% of the available flip-flops and lookup tables.

Multiple injection restriction

One assumption of the water injection controller based on residual fuel mass is that an early combustion follows a misfire or late combustion phasing when there is a high residual fuel amount. This is the case (when there is no water injection) shown in Figure 3. However, when water is added, there is the risk that the added water will completely extinguish the combustion. When this occurs, the fuel is not burnt but rather transferred to the subsequent cycle. In the water injection controller, the water injection amount is directly proportional

to the residual fuel mass which leads to an undesirable large water injection in the next cycle as shown in Figure 8.

This scenario has two possible outcomes. In the first, the desired one, the high residual fuel leads to combustion which is delayed by the added water and results in a return to the desired combustion phasing. In the second, the high amount of injected water leads to overcooling of the combustion chamber such that not enough thermal energy remains for the fuel to autoignite. Then the base controller design would continually increase the injected water amount as is the case in Figure 8. This leads to complete extinction of the HCCI combustion which then needs to be reignited by returning to the SI mode. This outcome leads to large amounts of water being injected into the cylinder and a large decrease in combustion stability and increased emissions.

To prevent the complete extinction of the HCCI combustion, the controller will only allow two consecutive water injections. This restriction can also decrease the combustion stability as some cycles which are very early may require water injection in subsequent cycles; however, this added restriction helps ensure that enough thermal energy will remain in the cycle following water injection to enable autoignition.

In-cycle control results

The feed-forward controller was tested at both optimal water injection timings on the SCRE with the primary goal of reducing the cyclic variation shown in Figure 1. The left-hand side of Figure 9 shows five cycles where the controller is not activated. Here the cyclic variation characteristic of the HCCI operation at the lean boundary is shown. Cycles 194 and 195 are stable cycles that are followed by a late combustion in cycle 196. This late inefficient combustion leads to a high residual fuel mass which is transferred to the subsequent cycle as shown in the calculation of residual fuel mass. Then, due to the high fuel mass and hot exhaust gas transferred to cycle 197, this leads to a rapid and early combustion. The high pressure rise rates blow away the thermal boundary layer which increases the heat transfer to the cylinder wall which in turn advances the combustion phasing of the following cycle 198.³⁹

The right-hand side of Figure 9 shows five engine cycles with the controller activated. Again cycles 719

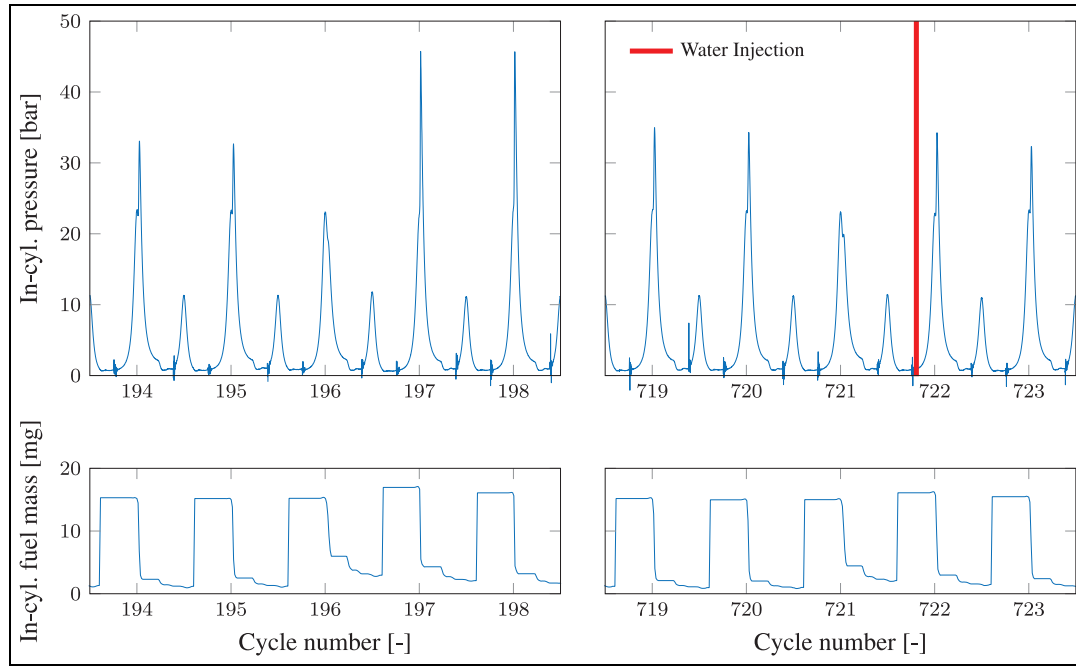


Figure 9. Left: In-cylinder pressure showing misfire after two stable cycles, followed by early rapid combustion when controller is not activated. Right: The same pattern as the left figure; however, control intervention of water injection prevents the early rapid pressure and restores combustion phasing to the desired value. In-cylinder fuel mass traces are also shown. Here, $n = 1500$ L/min, NVO = 150°CA , IMEP = 4.2 bar, $(p_{inj} - p_{cyl}) = 50$ bar and $SOI_{H_2O} = 580^\circ\text{CA}$.

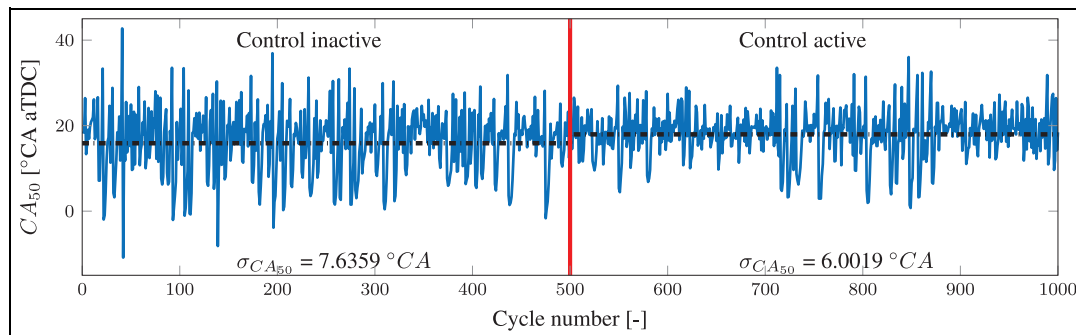


Figure 10. Combustion phasing, CA_{50} , stability improvement with in-cycle controller based on residual fuel mass at EVC. Controller is activated after 500 cycles. Here, $n = 1500$ L/min, NVO = 150°CA , IMEP = 4.2 bar, $(p_{inj} - p_{cyl}) = 50$ bar and $SOI_{H_2O} = 580^\circ\text{CA}$.

and 720 are stable cycles followed by a late combustion in cycle 721. In this case, the FPGA model calculates the increased residual fuel mass in the cylinder and is able to predict an early combustion phasing leading to a control input of water injection during the main compression to reduce the cylinder temperature. Here the control interaction effectively lowers the cylinder temperature which retards combustion phasing and lowers the pressure rise rate to the desired levels for cycles 722 and 723.

At a given engine speed load point, 1000 consecutive cycles were recorded and the controller was activated after the first 500 cycles. This is used to examine the performance of the controller on increasing combustion stability.

The performance of the controller at stabilizing the combustion phasing over 500 cycles is shown in Figure 10. Here the variation in combustion phasing after cycle 500 is reduced for both water injection timings after the controller is enabled. For the water injection at 580°CA aTDC, the standard deviation in combustion phasing is reduced from 7.64°CA to 6.00°CA aTDC or a reduction of 21.4% when the controller is enabled. The average CA_{50} is slightly retarded from 15.9°CA to 17.9°CA aTDC, but most of the cycles with a very early combustion phasing have been prevented, which helps stabilize the combustion overall as the number of very late combustion events has also been reduced.

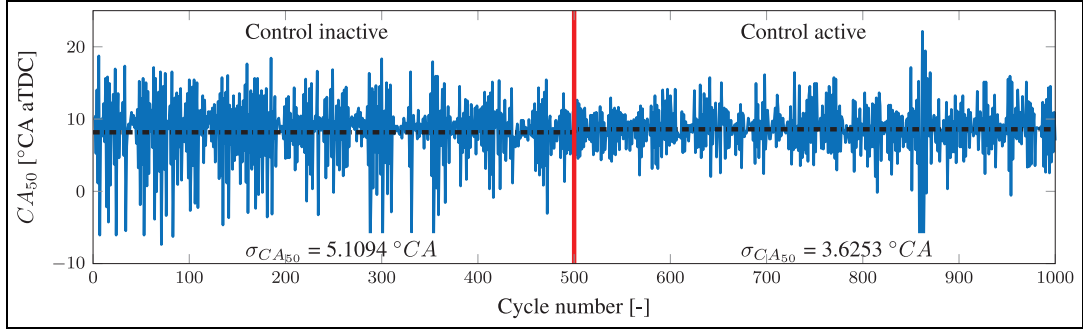


Figure 11. Combustion phasing, CA_{50} , stability improvement with in-cycle controller based on residual fuel mass at EVC. Controller is activated after 500 cycles. Here, $n = 1500$ L/min, $NVO = 185^\circ CA$, $IMEP = 2.4$ bar, $(p_{inj} - p_{cyl}) = 50$ bar and $SOI_{H_2O} = 270^\circ CA$.

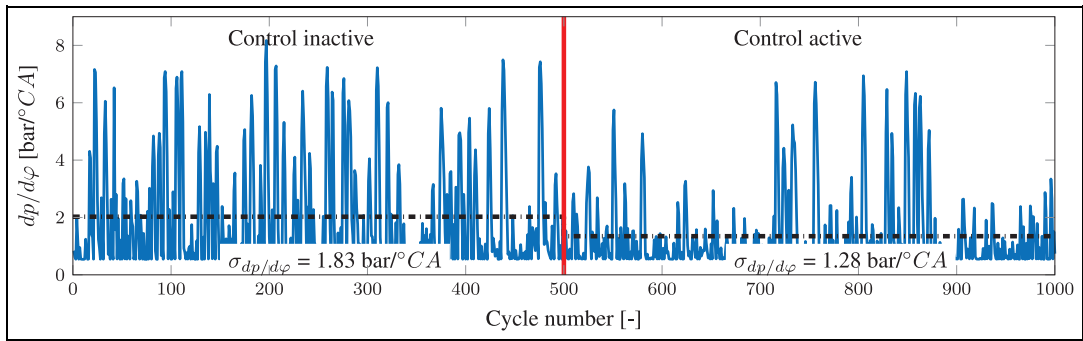


Figure 12. Maximum pressure rise rate, $dp/d\phi$, stability improvement with in-cycle controller based on residual fuel mass at EVC. Controller is activated after 500 cycles. Here, $n = 1500$ L/min, $NVO = 150^\circ CA$, $IMEP = 4.2$ bar, $(p_{inj} - p_{cyl}) = 50$ bar and $SOI_{H_2O} = 580^\circ CA$ aTDC.

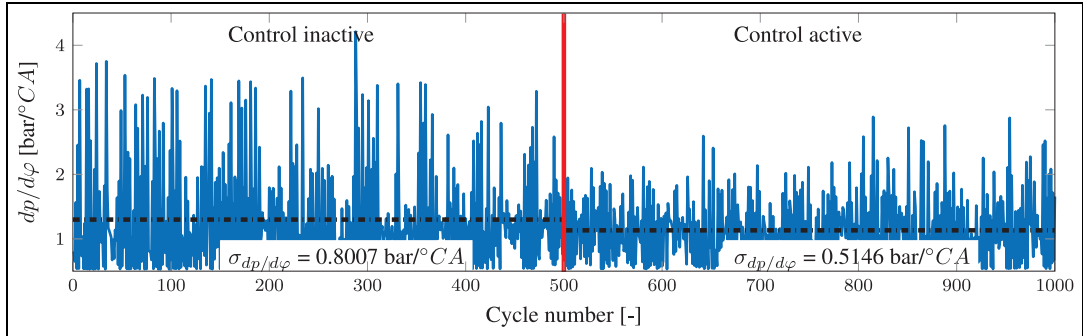


Figure 13. Maximum pressure rise rate, $dp/d\phi$, stability improvement with in-cycle controller based on residual fuel mass at EVC. Controller is activated after 500 cycles. Here, $n = 1500$ L/min, $NVO = 185^\circ CA$, $IMEP = 2.4$ bar, $(p_{inj} - p_{cyl}) = 50$ bar and $SOI_{H_2O} = 270^\circ CA$ aTDC.

A similar result can also be observed when the water injection takes place at $270^\circ CA$ aTDC, as the standard deviation in combustion phasing is reduced from $5.11^\circ CA$ to $3.63^\circ CA$ or a reduction of 29.0% (Figure 11).

Similar improvements can be seen for the peak pressure rise gradient of the same 1000 cycles as shown in Figure 12. Again, after the controller is activated, the number of cycles with a high pressure rise gradient is significantly reduced for both injection timings. A

reduction in the average pressure rise gradient from 2.02 to 1.72 bar/ $^\circ CA$ after the controller is enabled for the test with water injection at $580^\circ CA$ is observed. Similarly, when the water is injected at $270^\circ CA$, the average pressure rise gradient decreases from 1.30 to 1.13 bar/ $^\circ CA$ when the controller is activated (Figure 13). This significant reduction is important to reduce combustion noise and engine wear.

Figure 14 depicts a similar operating point to Figure 2 and shows the improvement in the

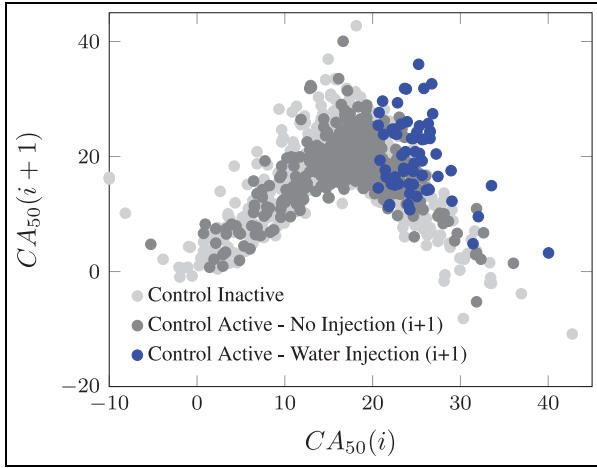


Figure 14. CA_{50} return map showing the improvement in combustion stability at NVO = 150 °CA, IMEP = 4.2 bar, and SOI_{H_2O} = 580 °CA aTDC.

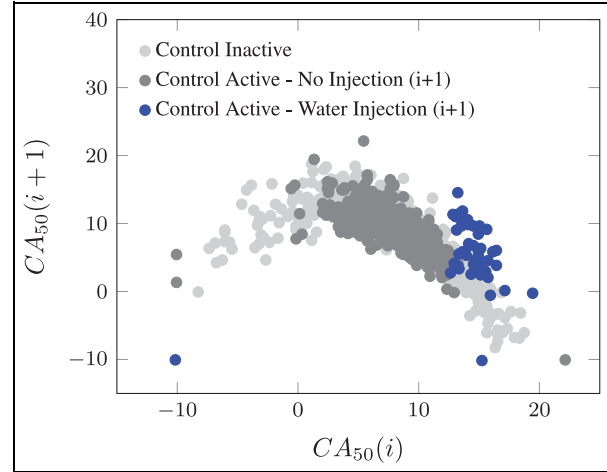


Figure 15. CA_{50} return map showing the improvement in combustion stability at NVO = 185 °CA, IMEP = 2.4 bar and SOI_{H_2O} = 270 °CA aTDC.

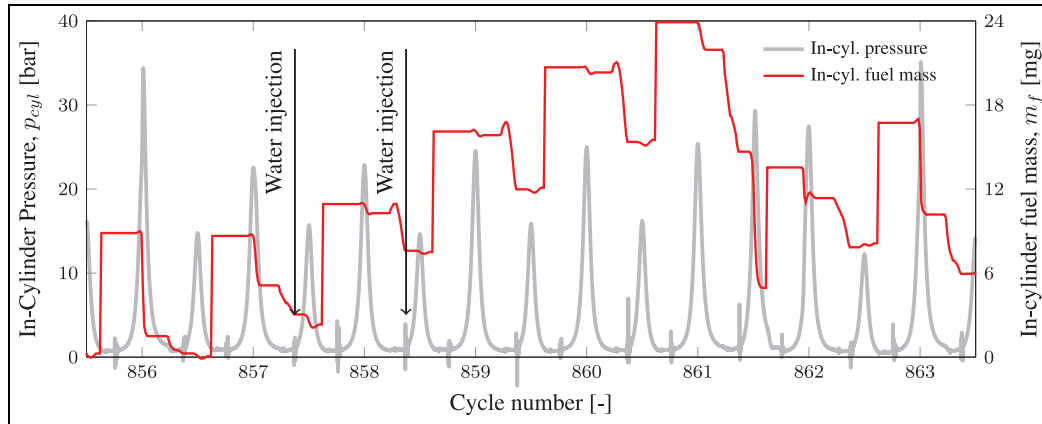


Figure 16. Additional cyclic instability due to control interaction at NVO = 185 °CA, IMEP = 4.2 bar and SOI_{H_2O} = 270 °CA aTDC.

combustion stability from the use of the residual fuel mass-based water injection controller. The stability improvement can be seen as the reduction of cycles located in the right leg of the CA_{50} return map. Not only are the extreme cycles completely eliminated, but the number of cycles outside the main point cloud is also greatly reduced.

The blue-colored points are directly influenced by the water injection controller in cycle $i + 1$. Here combustion phasing in the current cycle is not affected but the combustion phasing in the following cycle is retarded by water injection seen as an upward vertical shift in the figure. This “removes” the right leg of the return map. The reduction in the left leg is due to the prevention of an early combustion following an early combustion in the previous cycle. Using Figure 2 to clarify further, the controller would prevent cycle 2 which would also prevent cycle 3 by shifting the combustion phasing back into the stable central area. Overall, reducing the spread of the CA_{50} return map

indicates that with the controllers activated an improvement in combustion stability is achieved.

A similar improvement using the water injection controller for the case shown in Figure 14 is presented in Figure 15. Now, with an injection timing at 270 °CA aTDC, the cycles that have been altered using water injection timing are more tightly grouped showing that the injected water mass was more accurately calculated compared to the earlier injection timing.

At both water injection timings, the presence of some cycles remaining outside the central point cloud on the CA_{50} return map shows that the controller does have complete disturbance rejection and some cyclic variation still remains. This effect can also be seen in Figures 10–13 where a significant variation in CA_{50} and the pressure rise rate still occurs even when the controller is active. The early cycles with a high pressure gradient are due to the controller not accurately predicting an early combustion and therefore not adding water (the dark gray cycles in the right leg of Figure 14) or

Table 3. Combustion stability improvement due to residual fuel mass–based water injection controller.

SOI_{H_2O} (°CA)	IMEP (bar)		CA_{50} (°CA)		$\Delta\sigma_{IMEP}$ (%)	$\Delta\sigma_{CA_{50}}$ (%)	$\Delta dp/d\phi$ (%)	Control interactions (cycles)
Controller	Off	On	Off	On				
580	4.28	4.32	15.9	18.0	−11.2	−21.4	−33.5	63/500
580	2.39	2.41	8.6	8.9	−10.0	−14.6	−14.3	33/500
580	4.23	4.24	15.2	17.2	−9.3	−22.2	−28.5	34/500
580	2.38	2.38	8.6	9.1	−0.2	−20.6	−32.0	47/500
270	2.40	2.45	8.2	8.6	−22.0	−29.1	−12.7	49/500
270	2.80	2.96	8.3	9.9	−27.3	−33.5	−20.0	14/500
270	2.38	2.29	8.2	9.5	8.4	−10.1	−16.1	125/500
270	3.30	3.41	10.9	12.2	−13.5	−22.3	−17.2	69/500

IMEP: indicated mean effective pressure.

too little water mass added to the cycles (the blue points that remain in the right lower side of the return maps). There are also cases where too much water has been injected, thus resulting in a late combustion phasing and extremely low pressure rise rates (the blue points that appear in the right upper side of the return map). This overcooling due to water injection could also cause a misfire and result in a high transfer of fuel to the next cycle resulting in an early combustion phasing with very rapid combustion which is what the controller is trying to prevent.

Clearly, the simple linear model for relating residual fuel mass to the amount of water injected does not completely capture the complex dynamics of the system. Improvements could be perhaps made by incorporating non-linear effects of a short injection duration but there could be inherent limitations due to possible non-linear dynamics.

Water-induced misfire

Although the proposed water injection controller is able to improve the combustion stability overall, misfire cycles and subsequent very early combustion phasing cycles caused by the water injection still occur. For example, the controller reduced additional misfire cycles followed by a very early strong combustion in Figure 16. Here an incomplete combustion in cycle 857 leads to an increase in residual fuel mass leading to the injection of water. This water causes a misfire in the subsequent cycle (858) leading to a further increase in residual fuel. As previously discussed, this is a known problem with a controller strictly based on the residual fuel mass. To combat this the controller stops injecting water. However, three more misfire cycles occur leading to a very high in-cylinder fuel mass, which then ignites during the NVO period of cycle 861. This leads to the early combustion phasing in cycle 863.

By only allowing two consecutive water injection events, the number of occurrences of this pattern is reduced but not entirely eliminated. Only one possible way to improve the controller and eliminate this extinction of HCCI combustion is to couple the second

consecutive water injection with a late spark to ensure that there is combustion.

Operating point variation

The combustion stability improvement of using the real-time calculated fuel mass at various load points is summarized in Table 3. Overall, the current residual fuel mass–based water injection controller shows a significant improvement in the HCCI combustion stability when evaluating $\Delta\sigma_{CA_{50}}$, $\Delta\sigma_{IMEP}$ and $\Delta\sigma_{IMEP}$.

Over the range of operating points tested, all show a decrease in the standard deviation of CA_{50} and pressure rise gradient. An improvement in all the operating points, except one, shows a reduction in the standard deviation of IMEP. This experimentally demonstrates that the controller is able to reduce the cyclic variations present in HCCI combustion. The increase in IMEP when the controller is activated shows that the combustion efficiency is increased. This means that, with the same fueling and even with a slight delay in combustion phasing, the engine is outputting more work for the same input energy. This is highly desired as the controller not only reduces the cyclic variability but also improves the thermal efficiency over a range of operating points.

The controller works over a range of operating conditions while showing a decrease in the standard deviation of combustion phasing and power output. The controller was also effective in reducing the average pressure rise rates with control interventions in approximately 10% of the cycles. The water injection at 270°CA aTDC was more effective at reducing cyclic variations, while the later water injection timing of 580°CA aTDC has a larger impact on the average pressure rise rate. Overall, the residual fuel mass feed-forward controller using either of the water injection timings performed well with only slight differences.

Conclusion and future work

Based on a real-time calculation of residual fuel mass, the feed-forward controller was able to prevent the

early rapid combustion following a late combustion timing in the engine. The controller improved the combustion phasing stability as evidenced in the return maps using water injection to retard the combustion phasing of cycles following a late combustion. The controller was tested at several operating points and showed improvements in the standard deviation of combustion phasing and IMEP, along with the average pressure gradient. The control intervention occurs in approximately 10% of the cycles.

Two separate water injection timings, identified as having the greatest impact on the combustion phasing, were tested. It was found that water injection at EVC provided the strongest effect on reducing the pressure gradient, but only a very short calculation window is available for the calculation of residual fuel mass and injected water quantity. This limited calculation time meant that FPGA hardware was needed.

The combustion stability improved with the simple controller developed. Further improvement of the controller is possible by examining the possible non-linear relations along with water injection coupled with late spark and is the subject of our future work.






Declaration of conflicting interests

The author(s) declared no potential conflicts of interest with respect to the research, authorship and/or publication of this article.

Funding

The author(s) disclosed receipt of the following financial support for the research, authorship, and/or publication of this article: This research was performed as part of the Research Group (Forschungsgruppe) FOR 2401 "Optimization Based Multiscale Control for Low Temperature Combustion Engines," which was funded by the German Research Association (Deutsche Forschungsgemeinschaft (DFG)) and the Natural Sciences Research Council of Canada Grant 2016-04646. Partial funding from Future Energy Systems at the University of Alberta is also gratefully acknowledged.

ORCID iDs

David Gordon  <https://orcid.org/0000-0002-7999-8234>
 Christian Wouters  <https://orcid.org/0000-0002-2562-3146>
 Maximilian Wick  <https://orcid.org/0000-0001-5033-930X>
 Jakob Andert  <https://orcid.org/0000-0002-6754-1907>
 Charles Koch  <https://orcid.org/0000-0002-6094-5933>

References

1. Breitbach H, Waltner A, Landefeld T and Schwarz C. Lean-burn stratified combustion at gasoline engines. *MTZ Worldwide* 2013; 74(5): 10–16.
2. Langen P, Melcher T, Missy S, Schwarz C and Schünnemann E. Neue BMW Sechs- und Vierzylinder-Ottomotoren

- mit High Precision Injection und Schichtbrennverfahren. In: *28th Internationales Wiener Motorensymposium*, Vienna, 26–27 April 2007. Dusseldorf: VDI-Verlag.
3. Waltner A, Lückert P, Schaupp U, Rau E, Kemmler R and Weller R. Die Zukunftstechnologie des Ottomotors: strahlgeführte Direkteinspritzung mit Piezo-Injektor. In: *27th Internationales Wiener Motorensymposium*, Vienna, 27–28 April 2006, pp.24–43. Dusseldorf: VDI-Verlag.
4. Zhao H. *HCCI and CAI engines for the automotive industry* (Woodhead Publishing in Mechanical Engineering). Boca Raton, FL; Cambridge: CRC Press; Woodhead Publishing, 2007.
5. Guibert P, Morin C and Mokhtari S. Verbrennungssteuerung durch Selbstzündung. *MTZ: Motortechnische Zeitschrift* 2004; 65(2): 122–130.
6. Stan C and Guibert P. Verbrennungssteuerung durch Selbstzündung. *MTZ: Motortechnische Zeitschrift* 2004; 65(1): 56–62.
7. Adcock I. Ice breaker! Mazda's Skyactiv-X using SpCCI. *SAE Automotive Engineering*, 2017, <https://www.sae.org/news/2017/09/ice-breaker>
8. Maurya RK and Agarwal AK. Experimental study of combustion and emission characteristics of ethanol fuelled port injected homogeneous charge compression ignition (HCCI) combustion engine. *Appl Energ* 2011; 88(4): 1169–1180.
9. Haraldsson G, Tunestål P, Johansson B and Hyvönen J. HCCI combustion phasing with closed-loop combustion control using variable compression ratio in a multi cylinder engine. SAE technical paper 2003-01-1830, 2003.
10. Manofsky L, Vavra J, Assanis D and Babajimopoulos A. Bridging the gap between HCCI and SI: spark-assisted compression ignition. *SAE technical paper 2011-01-1179*, 2011.
11. Atkins MJ and Koch CR. The effect of fuel octane and diluent on homogeneous charge compression ignition combustion. *Proc IMechE, Part D: J Automobile Engineering* 2005; 219(5): 665–675.
12. Ghazimirsaeed A and Koch CR. Controlling cyclic combustion timing variations using a symbol-statistics predictive approach in an HCCI engine. *Appl Energ* 2012; 92: 133–146.
13. Lehrheuer B, Pischinger S, Wick M, Andert J, Berneck D, Ritter D, et al. A study on in-cycle combustion control for gasoline controlled autoignition. SAE technical paper 2016-01-0754, 2016.
14. Saxena S and Bedoya ID. Fundamental phenomena affecting low temperature combustion and HCCI engines, high load limits and strategies for extending these limits. *Prog Energ Combust* 2013; 39(5): 457–488.
15. Hellstrom E, Larimore J, Jade S, Stefanopoulou AG and Jiang L. Reducing cyclic variability while regulating combustion phasing in a four-cylinder HCCI engine. *IEEE T Contr Syst T* 2014; 22(3): 1190–1197.
16. Larimore J. *Experimental analysis and control of recompression homogeneous charge compression ignition combustion at the high cyclic variability limit*. PhD Dissertation, University of Michigan, Ann Arbor, MI, 2014.
17. Vaughan A. *Adaptive machine learning for modeling and control of non-stationary, near chaotic combustion in real-time*. PhD Dissertation, University of Michigan, Ann Arbor, MI, 2015.

18. Vaughan A and Bohac SV. A cycle-to-cycle method to predict HCCI combustion phasing. In: *ASME 2013 internal combustion engine division fall technical conference*, Dearborn, MI, 13–16 October 2013, pp.V001T03A026. New York: American Society of Mechanical Engineers.
19. Shahbakhti M and Koch C. Characterizing the cyclic variability of ignition timing in a homogeneous charge compression ignition engine fuelled with n-heptane/iso-octane blend fuels. *Int J Engine Res* 2008; 9(5): 361–397.
20. Ritter D, Andert J, Abel D and Albin T. Model-based control of gasoline-controlled auto-ignition. *Int J Engine Res* 2018; 19(2): 189–201.
21. Andert J, Wick M, Lehrheuer B, Sohn C, Albin T and Pischinger S. Autoregressive modeling of cycle-to-cycle correlations in homogeneous charge compression ignition combustion. *Int J Engine Res* 2018; 19(7): 790–802.
22. Nuss E, Ritter D, Wick M, Andert J, Abel D and Albin T. Reduced order modeling for multi-scale control of low temperature combustion engines. In: R King (ed.) *Active flow and combustion control 2018*. Cham: Springer, 2019, pp.167–181.
23. Morcinkowski B. *Simulative Analyse von zyklischen Schwankungen der kontrollierten ottomotorischen Selbstzündung*. PhD Dissertation, RWTH Aachen University, Aachen, 2015.
24. Ebrahimi K and Koch C. Model predictive control for combustion timing and load control in HCCI engines. SAE technical paper 2015-01-0822, 2015.
25. Choi S, Ki M and Min K. Development of an on-line model to predict the in-cylinder residual gas fraction by using the measured intake/exhaust and cylinder pressures. *Int J Automot Techn* 2010; 11(6): 773–781.
26. Pfluger J, Andert J, Ross H and Mertens F. Rapid control prototyping for cylinder pressure indication. *MTZ Worldwide* 2012; 73(11): 38–42.
27. Trajkovic S, Milosavljevic A, Tunestål P and Johansson B. FPGA controlled pneumatic variable valve actuation. In: *SAE 2006 world congress & exhibition*, Detroit, MI, 3–6 April 2006. Warrendale, PA: SAE International.
28. Wilhelmsson C, Tunestål P and Johansson B. FPGA based engine feedback control algorithms. In: *FISITA 2006 world automotive congress*, Yokohama, Japan, 22–27 October 2006. Tokyo, Japan: JSAE.
29. Wick M, Lehrheuer B, Albin T, Andert J and Pischinger S. Decoupling of consecutive gasoline controlled auto-ignition combustion cycles by field programmable gate array based real-time cylinder pressure analysis. *Int J Engine Res* 2018; 19: 153–167.
30. Gordon D, Wouters C, Wick M, Xia F, Lehrheuer B, Andert J, et al. Development and experimental validation of a real-time capable FPGA based gas-exchange model for negative valve overlap. *Int J Engine Res*. Epub ahead of print 24 July 2018. DOI: 10.1177/1468087418788491.
31. Eng JA. Characterization of pressure waves in HCCI combustion. In: *SAE powertrain & fluid systems conference & exhibition*, Toronto, ON, Canada, 16–19 October 2002. Warrendale, PA: SAE International.
32. Maurya RK. *Characteristics and control of low temperature combustion engines: employing gasoline, ethanol and methanol*. Cham: Springer, 2017.
33. Hellström E, Stefanopoulou A, Vavra J, Babajimopoulos A, Assanis DN, Jiang L and Yilmaz H. Understanding the dynamic evolution of cyclic variability at the operating limits of HCCI engines with negative valve overlap. *SAE Int J Engines* 2012; 5: 995–1008.
34. Merker GP, Schwarz C and Teichmann R. *Grundlagen Verbrennungsmotoren: Simulation der Gemischbildung, Verbrennung, Schadstoffbildung und Aufladung*. 4th ed. Wiesbaden: Vieweg + Teubner Verlag, 2009.
35. Woschni G. A universally applicable equation for the instantaneous heat transfer coefficient in the internal combustion engine. SAE technical paper 670931, 1967.
36. Chang J, Güralp O, Filipi Z, Assanis DN, Kuo TW, Najt P and Rask R. New heat transfer correlation for an HCCI engine derived from measurements of instantaneous surface heat flux. SAE technical paper 2004-01-2996, 2004.
37. Hohenberg G. *Experimentelle Erfassung der Wandwärme von Kolbenmotoren*. PhD Thesis, Universität Graz, Graz, 1980.
38. Soyhan H, Yasar H, Walmsley H, Head B, Kalghatgi G and Sorousbay C. Evaluation of heat transfer correlations for HCCI engine modeling. *Appl Therm Eng* 2009; 29(2–3): 541–549.
39. Tsurushima T, Kunishima E, Asaumi Y, Aoyagi Y and Enomoto Y. The effect of knock on heat loss in homogeneous charge compression ignition engines. In: *SAE 2002 world congress & exhibition*, Detroit, MI, 4–7 March 2002. Warrendale, PA: SAE International.